

# RBNN: Memory-Efficient Reconfigurable Deep Binary Neural Network with IP Protection for Internet of Things

Huming Qiu\*, Hua Ma\*, Zhi Zhang, Yifeng Zheng,

Anmin Fu, Pan Zhou, Yansong Gao, Derek Abbott, *Fellow IEEE*, and Said F. Al-Sarawi, *Member IEEE*.

**Abstract**—Though deep neural network (DNN) models exhibit outstanding performance for various applications, their large model size and extensive floating-point operations (FLOPS) render deployment on mobile computing platforms a major challenge, and, in particular, on Internet of Things (IoT) devices. One appealing solution is model quantization that reduces the model size and uses integer operations commonly supported by microcontrollers (MCUs usually do not support FLOPS). To this end, a 1-bit quantized DNN model or deep binary neural network (BNN) maximizes the memory efficiency, where each parameter in a BNN model has only 1-bit. In this paper, we propose a reconfigurable BNN (RBNN) to further amplify the memory efficiency for resource-constrained IoT devices. Generally, the RBNN can be reconfigured on demand to achieve any one of  $M$  ( $M > 1$ ) distinct tasks with the same parameter set, thus only a single task determines the memory requirements. In other words, the memory utilization is improved by  $\times M$ . Our extensive experiments corroborate that up to seven commonly used tasks ( $M = 7$ , 6 of these tasks are image related and the last one is audio) can co-exist (the value of  $M$  can be larger). These tasks with a varying number of classes have no or negligible accuracy drop-off (i.e., within 1%) on three binarized popular DNN architectures including VGG, ResNet, and ReActNet. The tasks span across different domains, e.g., computer vision and audio domains validated herein, with the prerequisite that the model architecture can serve those cross-domain tasks. To protect the intellectual property (IP) of an RBNN model, the reconfiguration can be controlled by both a user key and a device-unique root key generated by the intrinsic hardware fingerprint (e.g., SRAM memory power-up pattern). By doing so, an RBNN model can only be used per paid user per authorized device, thus benefiting both the user and the model provider.

**Index Terms**—Reconfigurable Binary Neural Network, Deep Neural Network, Quantization, IP Protection, Internet of Things.

Corresponding Author: Y. Gao.

H. Qiu and H. Ma contribute equally.

H. Qiu, is with School of Cyberspace Science and Engineering, Nanjing University of Science and Technology, Nanjing, China. e-mail: 120106222682@njjust.edu.cn.

H. Ma, S. Al-Sarawi, and D. Abbott are with School of Electrical and Electronic Engineering, The University of Adelaide, Adelaide, Australia. e-mail: {hua.ma;said.alsarawi;derek.abbott}@adelaide.edu.au

Z. Zhang is with Data61, CSIRO, Sydney, Australia. e-mail: zhi.zhang@data61.csiro.au.

Y. Zheng is with the School of Computer Science and Technology, Harbin Institute of Technology, Shenzhen, Guangdong 518055, China. e-mail: yifeng.zheng@hit.edu.cn.

P. Zhou is with Hubei Engineering Research Center on Big Data Security, School of Cyber Science and Engineering, Huazhong University of Science and Technology, Wuhan, 430074, Hubei, China. e-mail: panzhou@hust.edu.cn.

Y. Gao and A. Fu are with School of Computer Science and Engineering, Nanjing University of Science and Technology, Nanjing, China. e-mail: fuam@njjust.edu.cn.

## I. INTRODUCTION

Deep neural networks (DNNs) today have been explored to achieve various tasks such as computer vision, natural language processing, and speech recognition. With the trend of Machine learning as a Service (MLaaS), trained models are put onto the cloud to provide an inference service. However, many critical tasks (e.g., autonomous driving) require zero- or minimum-latency in the prediction or inference stage, thus the latency caused by the interaction between the cloud and user is a hurdle. In addition, when a model is hosted on the cloud, it is limited to a fixed level of network bandwidth that might not be always achievable. Further, hosting the model on the cloud poses a threat to data privacy, e.g. data must not leave the device. To achieve low-latency, reliable network connectivity, and privacy, a straightforward solution is to host the model on localized pervasive mobile computing platforms such as internet of things (IoT) devices.

However, a DNN model has a large number of parameters that are typically stored with a precision of `float32`, demanding a large model memory footprint. For instance, AlexNet [1] has more than one hundred parameters that can potentially result in a model size of 240 MB [2]. Such memory requirements can hardly be satisfied by memory-constrained devices. We note that FPGA is commonly utilized today for accelerating the inference while its on-chip memory can be as low as 10 MB [2]. Furthermore, floating-point operations (FLOPS) are numerous and computing-intensive. Take for example the ResNet-50 [3], which needs about 4.1B FLOPS to process an image size of  $224 \times 224$  [4]. The FLOPS are available in high-performance hardware such as GPUs but may not be (well) supported by low-power IoT devices such as drones and watches.

The above requirements of large model size and extensive FLOPS make the DNN models heavyweight and introduce notable latency to the model inference or prediction, thus hindering their ubiquitous deployment the IoT devices. As such, the model must be as lightweight as possible [5] when it is implemented in resource constrained computing platforms such as IoT devices. A practical solution is to reduce model precision by performing so-called *model quantization*. This approach has attracted significant attention from both academia [6] and industry [7].

### A. Limitations:

The model quantization can be classified into two categories based on where about the quantization is introduced: post-training quantization and training-aware quantization [7]. The former quantizes the weights and/or activation after the model has been trained and results in a slight degradation in the inference accuracy, which is usually applicable when quantizing heavyweight DNN models. If a model is designed to be lightweight in terms of IoT devices, then training-aware quantization improves accuracy, compared to post-quantization. The quantization of these models can range from 8-bit, 4-bit and even down to 1-bit [8]–[13] for not only weight but also activation [14]. Particularly, 1-bit quantized models are referred to as binary neural networks (BNNs) where both the weights and activations are represented by two possible values, -1/0 and +1, substantially reducing the memory footprints. In addition, the FLOPS are replaced by simpler operations such as the XNOR logical operation and Bitcount to expedite the inference [15].

To this end, *it seems that the memory efficiency for a given model is maximized by the binarized model*. We are now interested in the following research question:

Is it possible to further increase the memory utilization of a given BNN? If so, what evidence can be used to pragmatically demonstrate that?

### B. Our Solution

We propose a reconfigurable deep binary neural network (RBNN) to integrate various tasks into the same model, thus further improving the memory utilization and facilitating this network deployment on IoT devices. Our main insight is that multiple tasks can be concurrently learned during the training stage through proper objective functions. Thus, multiple tasks can be trained at the same time on the same model [16]. However, unlike common multi-task learning that shares representations among related tasks [16], the RBNN does *not* share representations and thus *can* train completely different tasks. By reconfiguring the parameters permutation, the RBNN can change the inference task on-demand to serve multiple purposes. Take autonomous driving as an example, we can train a face recognition task and a traffic sign recognition task in the same ResNet model of RBNN and both tasks share the same model parameters including weights and activations. In the inference stage, the trained model first serves the face recognition to authorize the driver and start the car and then switches to the traffic sign recognition task to discern traffic lights by parameters permutation. Given that a DNN model is of great commercial value to the model provider [17]–[19], the RBNN's reconfiguration property is a naturally appealing feature in this context. This is because the reconfiguration can be bounded with an authorized key from the model provider, which enables intellectual property (IP) protection on a trained model, that is, only a unique key can properly configure the model to a specific task.

### C. Contributions

Our experiments on RBNN are to answer the following research questions.

Q1: Can multiple distinctive tasks be co-learned during the training, thus enabling the RBNN?

Q2: Can tasks with varying numbers of classes/labels be compatible in the RBNN?

Q3: Can tasks from different domains co-exist in the RBNN?

Q4: Is the RBNN independent of model architectures?

Building upon the experiments designed for above questions, contributions of this work are threefold:

- 1) We propose RBNN to address memory constraints when deploying a DNN model onto IoT devices to achieve low-latency, low-network connectivity, and data privacy. Instead of training a BNN model for a single task, a single RBNN model can be reconfigured on-demand to serve multiple inference tasks.
- 2) We comprehensively evaluate RBNN on three common model architectures including VGG, ResNet, and ReActNet on seven commonly used datasets. We demonstrate that i) tasks with a varying number of classes can be integrated into the RBNN (Q2), ii) tasks from two different domains: vision and audio, can co-exist in the RBNN as the model architecture can handle cross-domain tasks (Q3). In addition, RBNN is independent on model architectures as validated via three varying model architectures (Q4). Our experiments show that RBNN achieves superior memory efficiency and the accuracy for each inference task in the RBNN is on par with its corresponding BNN (Q1).
- 3) We propose an IP protection framework to bind the RBNN reconfiguration with both *user key* and *device key* derived from a physical unclonable function (PUF) to prevent running the model on an unauthorized device, and enabling the IP license to be issued per device and per user.

The remainder of this paper is organized as follows. Section II gives the necessary background related to the presented work. Section III details the implementation of the proposed RBNN framework. Section IV comprehensively evaluates the RBNN with various model architectures and datasets. Section V exploits the reconfiguration to naturally protect the RBNN IP by binding the reconfiguration of each task by a unique key. Section VI demonstrates that abusing the multi-task for the backdoor attack is trivial to be defeated and experimentally validated. This work is concluded in Section VII.

## II. BACKGROUND AND RELATED WORK

### A. Deep Neural Network

When provided an input  $x \in \mathbb{R}^n$  with  $n$ -dimension, a DNN  $F_\theta$  will map to one of  $C$  classes in common classification tasks. More precisely, the output  $y \in \mathbb{R}^m$  of the DNN is a so-called softmax—a probability vector for  $C$  classes. In other words, the  $y_i$  is the probability that the input  $x$  belongs to the  $i_{\text{th}}$  class. An input  $x$  is inferred as class  $i$  if  $y_i$  has the highest probability, so that the output class label  $z$  is  $\operatorname{argmax}_{i \in [1, C]} y_i$  [20].

Generally, the DNN model  $F_\theta$  is trained with a number of samples with annotated ground-truth labels—training dataset. The trainable parameter  $\theta$  is comprised of weights and biases, which will be learned during the training phase. Specifically, suppose that the training dataset is a set,  $\mathcal{D}_{\text{train}} = \{x_i, y_i\}_{i=1}^S$  of  $S$  samples, where  $x_i \in \mathbb{R}^n$  and corresponding ground-truth labels  $z_i \in [1, C]$ . The training is to learn parameters that minimize the errors between inputs predictions and their ground-truth labels, which can be evaluated by a loss function  $\mathcal{L}$ . Parameters  $\Theta$  after training are expressed as:

$$\Theta = \operatorname{argmin}_{\Theta^*} \sum_i^S \mathcal{L}(F_\Theta(x_i), z_i). \quad (1)$$

Notably, to have accurate inference, the DNN always uses many layers. Thus, a huge number of parameters need to be trained and stored. In the inference stage, the computation and storage overhead are highly related to the size of the DNN model. In addition, the parameters are expressed with a precision of `float32` by default, so the inference is performed based on the intensive floating-point operations (FLOPS).

### B. Binary Neural Network

In the literature, a number of model compression techniques have been proposed to reduce the memory footprint and the computation overhead. Among these techniques (such as pruning for trimming off less important parameters [21], knowledge distillation for transferring knowledge from a large model to a small one [22]), and model quantization [23] is one of the most efficient solutions. Compared with a full-precision model that uses floating points, a quantized model compresses the original model weights by representing the model weights with lower precision while retaining the inference accuracy. The ultimate quantization is binarization, which results in the binary neural network (BNN), such approach can play a significant role in maximizing memory utilization for resource-constrained IoT devices.

Binarization is a 1-bit quantization, where a parameter has only two possible values, namely  $-1/0$  or  $+1$ . When training a BNN model, only 1-bit is used to represent both weight  $w$  and activation  $a$  parameters. Following [14], binary functions are expressed as follows:

$$Q_w(w) = \alpha b_w, \quad Q_a(a) = \beta b_a,$$

where  $b_w$  and  $b_a$  represent the binary weight and activation, and each is multiplied by a scale factor of  $\alpha$  or  $\beta$ . The sign functions of  $Q_w$  and  $Q_a$  for binarization are as follows:

$$\operatorname{sign}(x) = \begin{cases} +1 & x \geq 0 \\ -1 & \text{otherwise.} \end{cases} \quad (2)$$

After binarization, the floating-point convolution operation in forward propagation can be expressed as:

$$z = \sigma(Q_w(w) \otimes Q_a(a)) = \sigma(\alpha\beta(b_w \odot b_a)),$$

where  $\odot$  represents the vector inner product realized by bitwise XNOR and Bitcount operations, which can be performed more efficiently. Thus, binarization not only saves memory footprint but also makes computation much more efficient as floating points operations are replaced by bitwise operations.

### C. Backdoor Attack by Abusing Multi-task Learning

A backdoor attack introduces malicious behavior or task besides the main task for which the model is trained [20], [24]. In other words, a backdoored model essentially has multiple tasks: a main task and one or more backdoored tasks [24]–[27]. The model trained for two tasks will exhibit both normal and backdoor behaviors, where the backdoor behavior is activated by the so-called *trigger*—a secret known only to the adversary. While previous backdoored tasks share the representation with the main task, TrojanNet [26] is a new backdoor technique for full-precision models rather than BNN that abuses the multi-task learning property to make each backdoored task independent from the main task.

As summarized by Gao et al [24], the backdoor can also be used for good purposes such as watermarking for model IP protection [18], acting as a honey-pot for trapping and catching adversarial examples [28], and verification for data deletion requested by users who have contributed the data [29]. Our proposed RBNN turns the inherent multi-task property abused by the backdoor attack into a good use for resource-constrained IoT devices, i.e., improving memory efficiency of BNN-based models by embedding multiple tasks into a BNN model.

## III. RECONFIGURABLE DEEP BNN

### A. Overview

Fig. 1 presents an overview of our proposed reconfigurable deep binary neural network (RBNN). By rearranging the order of network parameters, the same network with the same parameters executes completely different tasks. This requires that multi-tasks be trained upon distinct datasets: each dataset corresponding to a specific task. Please note that the multi-task training in RBNN does not learn shared representation among similar tasks as previous reported [16], rather, it learns different representations specific to each task. Nonetheless, both cases leverage the high capacity or redundancy of the DNN. Below we elaborate on how to implement RBNN through binarization.

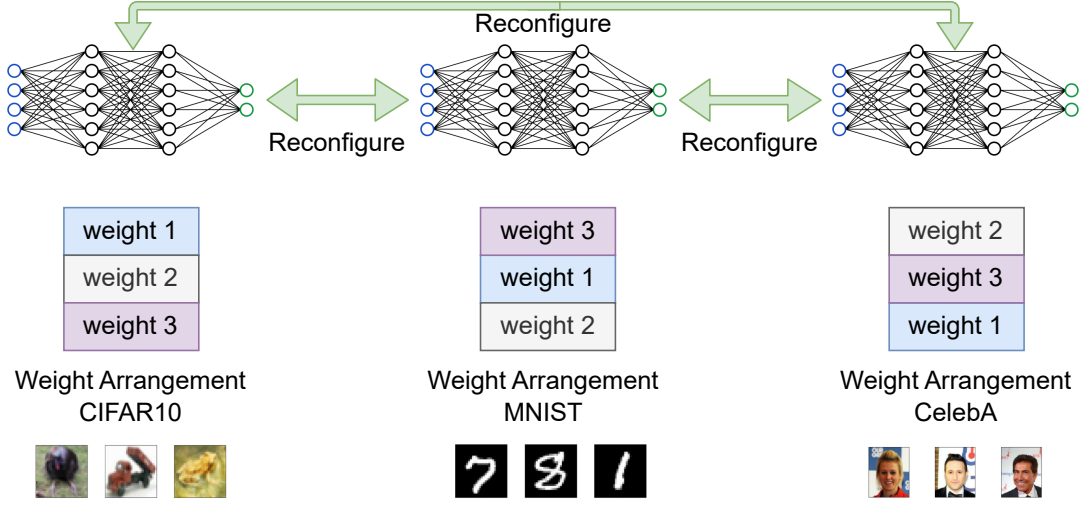


Figure 1: Overview of reconfigurable deep (binary) neural network. Rearranging the same network parameters (e.g., weight and activation) can switch to a network task from e.g., natural image classification on CIFAR10 to digit recognition on MNIST. Notably, the parameter rearrangement can be individually applied to *each* layer. The bidirectional arrow means that the *any two tasks* can be flexibly reconfigured from one to the other.

## B. Implementation

1) *Multi-Task Training*: The key insight of RBNN is to utilize the multi-task learning capability of DNN. Thus, different tasks  $\{T_1, T_2, \dots, T_M\}$  share the same parameter set including weights and biases. For convenience, we use  $T_m$  ( $m \in \{1, \dots, M\}$ ) to denote a network task. As illustrated in Fig. 1, each  $T_m$  can be immediately switched on by reconfiguring the network parameter orders (i.e., parameter permutation).

Suppose that a dataset  $D_m$  is used to train  $T_m$  and  $(x_i^m, y_i^m)$  denotes the  $i$ -th sample from  $D_m$ . The overall loss  $L$  (see loss description in Eq 1) of the multi-task training is the summation of individual task losses, which can be expressed as below:

$$\begin{aligned}
 L &= \sum_{m=1}^M \underbrace{L_{T_m}(T_m(x_i^m), y_i^m)}_{L_{T_m}} \\
 &= \underbrace{L_{T_1}(T_1(x_i^1), y_i^1)}_{L_{T_1}} + \dots + \underbrace{L_{T_M}(T_M(x_i^M), y_i^M)}_{L_{T_M}}.
 \end{aligned} \tag{3}$$

The overall loss  $L$  can be optimized with gradient descent on  $w_{T_m}$  and its gradient is given by:

$$\frac{\partial L}{\partial w} = \sum_{m=1}^M \frac{\partial L_{T_m}}{\partial w_{T_m}}. \tag{4}$$

The crucial step is to reconfigure the  $w$  to fit  $T_m$  and obtain  $L_{T_m}$ . This can be achieved by permutation, for example  $w_{T_2} \leftarrow \text{Reconfig}(w_{T_1})$  by reconfiguring the same parameters through permutation. In principle, we can train an arbitrary number of distinct tasks by the parameter permutations. In Eq. 3, the importance of each task is equal, thus the regularization is same. Alternatively, we can use a distinct regularization factor for each  $L_{T_m}$  to reflect the distinct importance of  $T_m$  if needed.

Intuitively, we can store the permutation or the corresponding mask that corresponds to a task to facilitate the reconfiguration of **Reconfig**. However, this could introduce a non-negligible memory overhead. To address this issue, we customize the approach from [26] and generate the **Reconfig** in the RBNN. Specifically, the tasks are reconfigured through distinct keys: each task is bounded to a specific key (i.e.,  $k_m$ ). Here,  $k_m$  is used as the seed of  $H$  (denoting a pseudo-random generator), where the parameters will be permuted by a pseudo-random output or sequence. Please note that the seed fed into  $H$  for each network layer should be distinct, resulting in a different reconfiguration for each layer. To do so,  $k_m$  (seed for the first layer) is passed through a recursive function to gain seed or key for the  $H$  of the next layer.

In this way, **Reconfig** is associated with  $k_m$ . As such,  $w_{T_m} \leftarrow \text{Reconfig}(w, k_m)$ . A byproduct is that  $w_{T_m}$  can only be configured correctly with a valid  $k_m$ . If an invalid key is applied, the parameters in the network will be wrongly permuted, causing the neural network to malfunction. To this end, the reconfiguration with valid keys issued from the model provider can provide IP protection to the network (see details in Section V).

As in Eq. 3, reconfigurable training requires training multiple different datasets in the same neural network. After training one batch of one dataset, we train a data batch from the next dataset. When training alternates with dataset batches,  $k_m$  is reconfigured to feed into  $H$  and transform  $w$  to  $w_{T_m}$  so that  $w_{T_m}$  corresponds to  $D_m$  for  $T_m$ .

2) *RBNN Training*: When training an RBNN model, the backpropagation algorithm based on gradient descent can be used directly to update the parameters [8], [14]. However, the binarization function such as the *sign* function in Eq. 2 is usually not differentiable. Even worse, the derivative value of part of the function disappears, and the derivative of the function is almost 0 everywhere, which is obviously incompatible with backward propagation.



Table I: Datasets Summery

Dataset	# of labels	Image size	# of samples (train; test)
MNIST [31]	10	$28 \times 28 \times 1$	70,000 (60,000; 10,000)
Fashion-MNIST [32]	10	$28 \times 28 \times 1$	70,000 (60,000; 10,000)
SVHN [33]	10	$32 \times 32 \times 1$	99,289 (73,257; 26,032)
CIFAR10 [34]	10	$32 \times 32 \times 3$	60,000 (50,000; 10,000)
CIFAR100 [34]	100	$32 \times 32 \times 3$	60,000 (50,000; 10,000)
CelebA [35]	2	$218 \times 178 \times 3$	182,732 (162,770; 19,962)
Speech Command (SC) [36]	35	$32 \times 32 \times 1$	95,394 (57,294; 38,100)

Thus, the original gradient descent based backward propagation cannot be immediately used for updating the binarized weights. We solve this issue by using a pass-through estimator (STE) in backward propagation [30]. The derivative of STE can also be represented as the propagation gradient through the hard tanh, which is defined as:

$$\text{Htanh}(x) = \text{clip}(x, -1, 1) = \max(-1, \min(1, x)). \quad (5)$$

By applying the hard tanh activation function, the RBNN model can now be directly trained using the gradient descent that is same when training the full-precision models. Nonetheless, if the absolute value of the full-precision activation is larger than 1, the  $\text{Htanh}(x)$  cannot be updated in backward propagation. Therefore, the identity function (i.e.,  $f(x) = x$ ) is also chosen to approximate the derivative of the *sign* function in practice.

#### IV. EXPERIMENTS

The experiments are designed mainly to answer the questions listed in Section I. We consider 7 popular datasets (Q1) corresponding to six computer vision domain tasks and one audio domain task (Q2). The number of classes for each task ranges from 2 to 100 (Q3). We use 3 common but different model architectures (Q4) for a comprehensive evaluation.

##### A. Setup

1) *Datasets*: There are 6 image datasets under vision domain and 1 speech recognition dataset under audio domain, as summarized in Table I. We then demonstrate that those different domain tasks can be reconfigured as long as the same model architecture can handle these tasks.

**MNIST/Fashion-MNIST**: The MNIST has handwritten digits of 10 classes by different people [31]. Fashion-MNIST dataset [32] is composed of 10 types of fashion products. Both contain 60,000 samples for training and 10,000 samples for testing. Each sample image is a gray-scale or single channel image with the size of  $28 \times 28$  pixels.

**SVHN**: This dataset is composed of street view house numbers from Google [33]. The training set contains 73257 samples and the test set contains 26,032 samples. Each gray-scale image is with the size of  $32 \times 32$ . Similar to MNIST, the SVHN is also a digital recognition dataset, but more difficult to recognize because of natural scenes.

**CIFAR10/100**: Both CIFAR10 and CIFA100 are natural color image datasets, with CIFAR10 and CIFAR100 having 10

and 100 classes, respectively [34]. The training set and the testing set of both CIFAR10 and CIFAR100 contain 50,000 and 10,000 images respectively. The CIFAR100 is harder to recognize than CIFAR10 due to the increased number of classes and decreased number of training samples per class.

**CelebA**: This dataset contains large-scale face attributes with more than 200K celebrity images, each with 40 attribute annotations [35]. The images in this dataset cover large pose variations and background clutter. CelebA has large diversities, large quantities, and rich annotations, including 10,177 identities, 202,599 face images, and 5 landmark locations, 40 binary attributes annotations per image. In our work, the training set and the testing set are divided according to the list\_eval\_partition.txt file in the dataset—we do not use validation set in this file. The training and testing sets have 162,770 and 19,962 samples, respectively. We have selected the gender attribute as a binary classification problem to train the model.

**Speech Command (SC)**: This audio dataset has spoken words designed to help train and evaluate keyword spotting systems [36]. It consists of 105,829 utterances of 35 words. Each utterance is stored as a one-second (or less) WAVE format file, with the sample data encoded as linear 16-bit single-channel PCM (Pulse-code modulation) values, at a 16 kHz rate. WAVE format files with a duration of less than one second are not used by us—these samples are excluded. As a consequence, a total of 95,394 audio data is left and randomly selected. 60% is used as the training set, and the rest is the testing set. Before feeding into the model, the Mel-Frequency Cepstral Coefficients (MFCC) is used to extract speech features and convert them into a frequency spectrum. The sampling rate is set to 6300 in order to convert the audio data format to  $32 \times 32 \times 1$ , and the mono data is copied to convert it into three channels.

2) *Model Architecture*: We consider binarizing three types of DNNs: ResNet18 [3], VGG [37] and ReActNet (using ResNet14 as backbone) [38] for experimental validations. ReActNet is a newly devised BNN framework to boost the BNN inference accuracy. It keeps the fully connected layers with full-precision representation by design, which we have followed. In addition, the backbone of ReActNet in our work is ResNet14, where the last block of ResNet18 is removed. This setting is to test whether the smaller model’s redundancy still supports the reconfiguration without accuracy drop when multiple tasks are simultaneously learned.

For the VGG model, the architecture is  $\text{conv}(128) \rightarrow \text{conv}(128) \rightarrow \text{conv}(256) \rightarrow \text{conv}(256) \rightarrow \text{conv}(512) \rightarrow \text{conv}(512) \rightarrow \text{fc}(1024) \rightarrow \text{fc}(1024) \rightarrow \text{fc}(\text{number of classes})$  where  $\text{conv}()$  is a convolutional layer with  $3 \times 3$  kernel size, and  $\text{fc}()$  is a fully connected layer. For the ResNet model, the specific ResNet18 is used. For both VGG and ResNet models, all convolutional layers and fully connected layers are binarized, and a batch normalization layer is added before the activation layer and after the fully connected layer. For the ReActNet model, the ResNet14 model is used as the basic skeleton of the network. The ReActNet by design reserves fully-connected layer to be represented with full-precision weights instead of

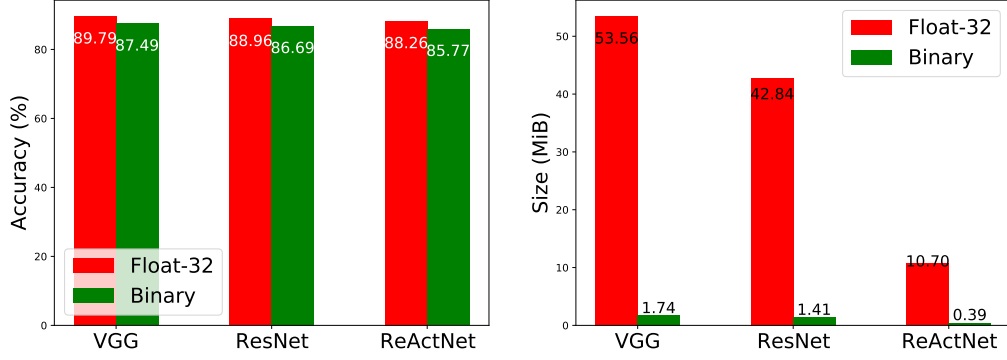


Figure 2: (Left) Testing accuracy of full precision model and BNN model of the same architectures. (Right) Model size of full precision model and BNN model of the same architectures.

being binarized. For all three models, the ADAM optimizer is used. The batch size is 256. We train all tasks with 100 epochs. The initial learning rate is  $5e-3$ , which decreases to  $1e-3$  at the 40th epoch and  $5e-4$  at the 80th epoch.

We sequentially integrate six tasks under image domain (MNIST, Fashion-MNIST, SVHN, CIFAR10, CelebA, CIFAR100) to train each of the abovementioned model architectures to verify the RBNN performance. In addition, we have added one more audio task, SC, when training the RBNN with ReActNet. This is to demonstrate the practicality of co-learning tasks from different domains as long as the specific model is capable of handling those tasks. The switch of each seven tasks is controlled with a distinctive key. In this way, the specific task can be configured immediately by using its key during the inference phase.

3) *Input Size Alignment*: The image size of different classification tasks differs, see Table I. For all the model architectures studied in this work, the model accepted image size is  $32 \times 32$ . In this context, for image size that is unequal to  $32 \times 32$ , we resize it to the model accepted input size. In addition, the model input image uses three channels by default. Therefore, for images, e.g., MNIST, SVHN as well as the spectrum of SC, with a single channel, we have firstly transformed them into three channels<sup>1</sup> before feeding them into the models.

## B. Experimental Results

1) *Baseline*: To set a baseline, we represent the model parameters with full precision (float32) and 1-bit, respectively, and choose to train the CIFAR10 using all these model architectures.

**Accuracy Comparison between Full-precision and 1-bit Model:** Results are detailed in Fig. 2. It is under expectation that the BNN model accuracy is slightly lower (around 2%) than the full precision model. This accuracy drop is similar with other works (see a summary in Table III of [14]). Notably,

<sup>1</sup>The command of `torchvision.transforms.Grayscale(3)` is used. In our case, this means that the single-channel image is replicated into a three-channel image.

the focus of this work is not to optimize the BNN accuracy itself—for instance, one can exploit Neural Architecture Search in the binary domain [39] for doing so, we are to integrate multiple BNN tasks by sharing the same model parameter set. Our concern is whether adding more tasks will greatly affect the accuracy of the task. Once the baseline of the BNN accuracy is optimized, our RBNN will naturally inherit the accuracy optimization benefit.

**Model Size Comparison between Full-precision and 1-bit Model:** The number of parameters of VGG, ResNet18 and ResNet 14 are 14.03M, 11.18M, and 2.78M, respectively<sup>2</sup>. There is about  $30\times$  model size reduction as a result of using the BNN model in comparison to its full precision model counterpart. For instance, the full precision model size of the VGG is up to 53.56MiB, while its BNN model size is only 1.74MiB. This demonstrates the advantage of employing BNN when the storage memory is limited.

**Accuracy Baseline of Individual Task with 1-bit Model:** The baseline accuracy of each task individually trained by each of three models are summarized in Table. II. The testing accuracy is evaluated after 100 epochs of training—further increase in the number of epochs did not result in noticeable improvement in the accuracy in our experiments. The accuracy reported in Table. II serves as the baseline when comparing with the accuracy of each task in the RBNN when multiple tasks are concurrently trained.

Here, we can see that the ReActNet has the best accuracy for the same task even though it is with the smallest model size. This is due to the fact that ReActNet is an optimized BNN framework that retains the full-precision representation for the fully-connect layers to maintain the model accuracy, in contrast the other two networks that use binary representation through the whole network.

2) *RBNN Performance*: Here, we sequentially add individual task one-by-one into the RBNN to see how and to which extent the number of tasks will affect individual task’s accuracy. Comprehensive results are detailed in Figure. 4 for VGG, Figure. 5 for ResNet18, and Figure. 6 for ReActNet.

<sup>2</sup>The model size is reported by `larq` library [40]

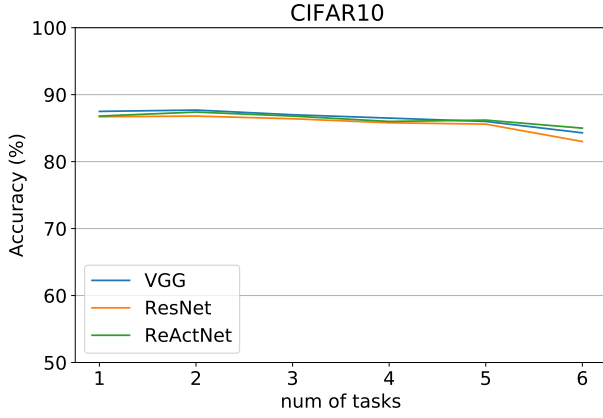


Figure 3: The accuracy of CIFAR10 task (it serves the first task integrated) when more other tasks are sequentially added into the RBNN.

Table II: Testing accuracy when each task/dataset is individually trained with a BNN model.

Model Architect.	Task/Dataset	BNN Accuracy (Baseline)
VGG	CIFAR10	87.49%
	MNIST	99.21%
	Fashion	94.57%
	SVHN	95.18%
	CelebA	97.25%
	CIFAR100	57.30%
ResNet18	CIFAR10	86.69%
	MNIST	99.12%
	Fashion-MNIST	94.09%
	SVHN	94.71%
	CelebA	96.29%
	CIFAR100	54.76%
ReActNet (ResNet14 as backbone)	CIFAR10	86.81%
	MNIST	99.31%
	Fashion-MNIST	94.14%
	SVHN	95.25%
	CelebA	97.11%
	CIFAR100	55.94%
	SC	93.04%

Corresponding to each concerned **question (Q)**, we have the following observations.

As for **Q1**, based on experiments with up to 7 tasks, it is clear that multiple tasks can be embedded in the same BNN model, thus corroborating the RBNN. In addition, the accuracy of each task in RBNN is similar the trained alone task—this accuracy difference is less than 1% in most cases. This is also exemplified in Figure 3 by the accuracy change of CIFAR10 task (it is the first task added) when more tasks are sequentially integrated.

As for **Q2**, the answer is affirmative. According to Table I, CelebA task is with 2 classes, SC task is with 35 classes, CIFAR100 task is with 100 tasks, and all the rest four tasks are with 10 classes. Therefore, the number of classes of each task varies greatly from 2 to 100. Overall, these tasks can co-exist with negligible accuracy drop. The worst accuracy drop occurs

Table III: Testing accuracy when two tasks are integrated under varying quantization width.

Model	Task	1-bit Quant. Acc. (B;R)	4-bit Quant. Acc. (B;R)	8-bit Quant. Acc. (B;R)
ResNet18	CIFAR10	(86.69%; 84.57%)	(89.26%; 88.42%)	(88.92%; 88.62%)
	CIFAR100	(54.76%; 54.55%)	(58.07%; 58.34%)	(57.11%; 57.76%)

(B;R): B means baseline accuracy when the task is *individually* trained; R means when multiple tasks are *co-learned*, standards for reconfiguration.

when the CIFAR100 is added, as it has the largest discrepancy with all other tasks in term of the number of classes. For instance, in the ResNet18, the CIFAR10 accuracy drops by about 2.8% when the number of tasks increases from 5 to 6 (the sixth task is CIFAR100). At the meantime, Fashion-MNIST, SVHN see an accuracy drop of about 1%. Evaluations on VGG and ReActNet model architectures demonstrate similar tendency. Notably, the accuracy drop of other tasks when CIFAR100 is added is minimal for the ReActNet, the potential reason lies on the fact that ReActNet i) is delicately designed for BNN, and ii) has full-precision presentation of the full-connected layers. The later could be the main reason affording a better compatibility of tasks with varying number of classes.

As for **Q3**, we have added the SC task as an audio domain task that is distinct from image classification of all other six tasks. The results are shown in Fig. 6 using the ReActNet. When SC is added, the accuracy drop of other 6 image tasks is negligible, while the SC itself accuracy drop is about 1% and thus also unnoticeable. Therefore, it is reasonable to conclude that the RBNN is able to learn tasks across different domains as long as the same model architecture can be used to these domains. This appears to be promising in practice as using same model architecture for cross-domain tasks is efficient. For instance, the transformer that achieves significant success in natural language processing, recently has demonstrated great potential in image-domain tasks [41] and GAN-domain tasks [42].

As for **Q4**, based on the experiments for three distinct model architectures, it is reasonable to conclude that the RBNN is generic to model architecture, regardless whether the model itself is specifically designed for BNN. Noting the VGG and ResNet are not delicate for BNN, while only the ReActNet is.

3) *Increase Quantization Width*: Though our main focus is BNN, here we extend the reconfiguration to other quantization width, in particularly, with 4-bit and 8-bit quantization<sup>3</sup>. We use ResNet (in particular, ResNet18) with two tasks of CIFAR10 and CIFAR100 for the extensive experiments in this part as ResNet is the most popular model architecture. We note that CIFAR100 has the largest number of classes. All other settings including learning rate and number of epochs are similar to the one reported in Section IV-A2.

<sup>3</sup>2-bit quantization exhibits unexpected lower accuracy, e.g., 50% on CIFAR10 dataset trained by ResNet18. We note that our focus is BNN. This paragraph shows that our proposal is also applicable to other quantization width (including 2-bit quantization) for some device with relatively larger memory size.

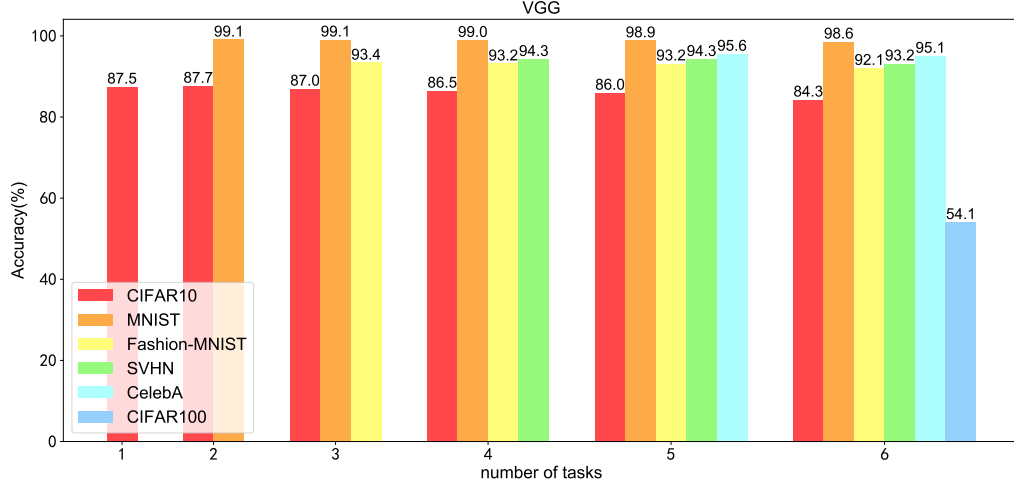


Figure 4: Testing accuracy of each individual task as the number of tasks increases. The VGG model is evaluated. Each task is sequentially added during the RBNN co-training processing.

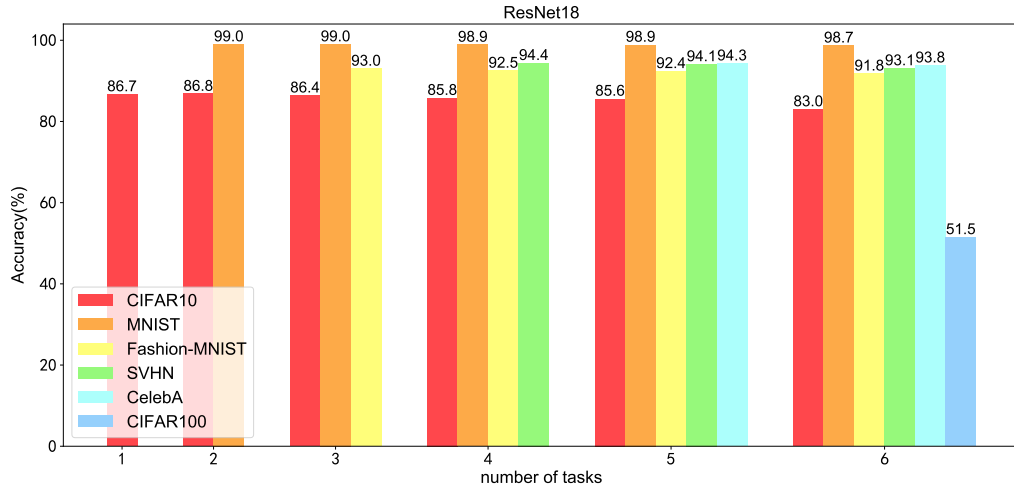


Figure 5: Testing accuracy of each individual task as the number of tasks increases. The ResNet18 model is evaluated. Each task is sequentially added during the RBNN co-training processing.

As can be seen from Table III the higher quantization width the better the accuracy of each task. In our experiments, for both 4-bit and 8-bit quantizations, the CIFAR10 has been improved by more than 2%, which is already comparable to the full-precision model accuracy, see Figure 2. For CIFAR100, it increases by more than 3%. In addition, we can see that the accuracy drop is minimized when a given task is co-learned in comparison with learned alone.

This further validates the proposed reconfiguration and its generic nature, which application is not solely limited to the concentrated BNN. Therefore, if the device has extra memory resources, then a slightly wider quantization approach can be used to improve the accuracy.

## V. IP PROTECTION

The IP protection of a DNN model is demanded in practice [17]–[19]. This is mainly because DNN models are usually trained with substantial computational resources that process vast amounts of proprietary data. The trained model is valuable for model provider as an IP and needs to be protected to preserve competitive commercial advantage [19].

It is recognized that the reconfiguration is naturally enabling model IP protection, e.g., allowing user for trial and to only pay per the task needed. For instance, the default task is provided to the user for trial before payment. The trial task has partial functionality, e.g., classifying a limited number of classes. Once the user is satisfied with the trial and pays for the license, the model provider sends a key to the user,  $User\_key_M$ , to reconfigure and thus unlock the task with a full



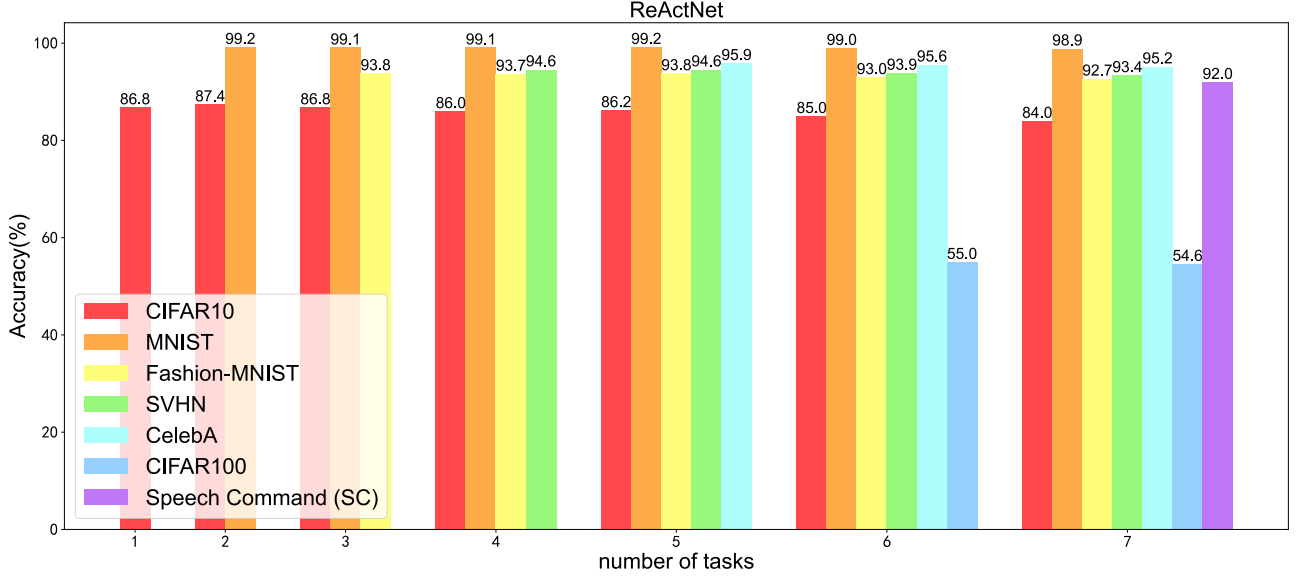


Figure 6: Testing accuracy of each individual task as the number of tasks increases. The ReActNet (ResNet14 as backbone) model is evaluated. The SC task is an audio domain task that is distinct from all other 6 tasks from image domain.

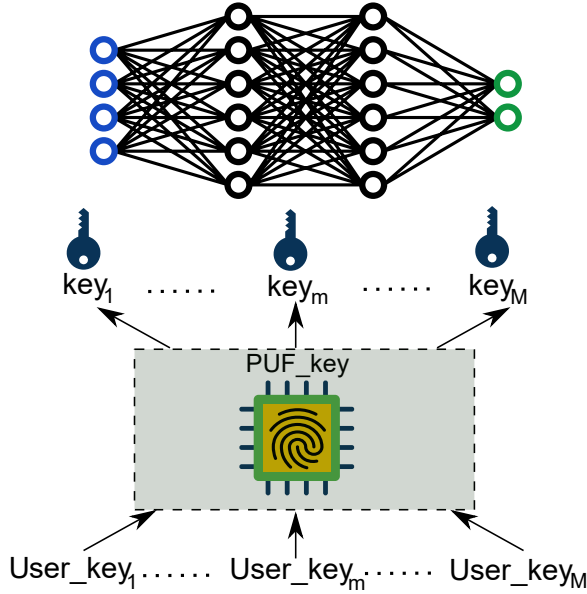


Figure 7: The  $key_M$  that reconfigures the model into the  $M_{th}$  task is a function of both the  $User\_key_M$  and the  $PUF\_key$ . The  $PUF\_key$  is extracted from the PUF alike ‘fingerprint’, thus uniquely bounded to each hardware device.

functionality. Notably, we have shown that tasks with varying number of classes can be effectively co-existed in RBNN. This scheme facilitates the user experience while protecting model provider IP. As for the user, she only needs to pay the task  $T_m$  that she is interested to save budget. Next we propose a scheme to allow the user pay not only per task but also per device.

Here, we propose to bind the key reconfiguring distinguish-

ing task with a unique device key that is extracted from the physical unclonable function (PUF) [43], [44]. In general, the PUF is akin the *fingerprint* of the device, such fingerprint can be converted into a usable cryptographic key,  $PUF\_key$ . The PUF is a result of inevitable and uncontrollable manufacturing variations, thus preventing forging two identical PUF instances even under the same manufacturing process. So that the  $PUF\_key$  is uniquely bounded with each device, which is hard to be physically cloned and replaced. Here, we can consider employing the intrinsic SRAM PUF to extract the  $PUF\_key$ , since the SRAM is pervasively embedded within commodity electronics, requiring no additional hardware modification. The details of extracting  $PUF\_key$  from (even low-end) commodity electronics in a lightweight manner can be referred to [45].

One prominent advantage of this  $PUF\_key$  enabled reconfiguration is that the payment now can be made per device, and even per task. For the former, the model provider can use the same  $key_m$  to reconfigure the same task for avoiding training the RBNN per device. From the user’s perspective, the  $User\_key_m$  is still different per device as the  $key_m$  is also a function of the  $PUF\_key$  that is unknown, as illustrated in Fig. 7. So that the provider can issue different  $User\_key_m$  to different device given the same task. Here, we can simply set  $key_m = \text{XOR}(User\_key_m, PUF\_key)$ —admittedly, other means of deriving  $key_m$  upon  $User\_key_m$  and  $PUF\_key$  can be adopted.

As for the later, the user can choose to only pay for a specific task  $T_m$ . If later another task is needed, the user can request from the model provider to issue a  $User\_key_m$  for the task of interest. In either case, the issued  $User\_key_m$  can not be used on other devices even that every device has been provided all tasks by the model provider. However, without knowing the  $User\_key_m$  specific to the device in-hand, the user cannot activate the task on the device, which protects the IP of the provider not only per device but also per task. At the same

time, this allows the user only pay for the task of interest on that device.

## VI. FLIP-SIDE OF TROJANNET AND ITS REMOVAL

Here, we show how our RBNN exploits the multi-task learning capability actually turned an adversary attack, in particular backdoor attack that abuses such capability, into an asset for model provider. In addition, we demonstrate that the attack TrojanNet [26]—closely related to ours from the *multi-task learning aspect*—can be easily defeated.

It has been shown that backdoor attack in principle abuses multi-task capability of the DNN model. To the best of our knowledge, only two works [25], [26] have explicitly demonstrated that the backdoor tasks could be more than one—all other works insert a single backdoor task into the main task. In contrast to the work by [25] and [26], our focus is more related to TrojanNet [26]. The TrojanNet is a model backdoor attack to embed or hid a secret task or multiple secret tasks into a default benign model. TrojanNet attack can naturally bypass a number of backdoor inspection countermeasures such as Neural Cleanse [46], DeepInspect [47]. This is because the default model under inspecting is benign and indeed containing no backdoor. The TrojanNet switches to the insidious task by invoking a secret key that is known to the attacker. In fact, it is non-trivial to invoke the key. Guo *et al.* [26] assume the TrojanNet is used along with a Trojan horse software, where the software switches the model into the secret task during loading time or at run-time when the key is activated. It appears that inserting a Trojan horse software, to a large extent, is a strong assumption. In addition, invoking the secret key on-demand is uneasy in practice, especially considering the network is disabled or/and secure protection mechanism is properly enabled. Moreover, the secret task is completely different from the main task expected by the user once the model task is switched, which is noticeable. As acknowledged by Guo *et al.* [26], the output size (number of labels) of main task shall be larger than the secret task, preferably to be equal. If the output size of main task is smaller than the secret task, it is suspicious due to the unexpected output size.

Nonetheless, here we propose an efficient TrojanNet removal technique as a countermeasure via just a simple fine-tuning. In particular, we consider training the main task for a number of epochs. This process does not hurt the accuracy of the main task at all, rather sharply disrupts hidden tasks. The reason is that the hidden task of TrojanNet does not share feature representations with the main task, which is different from other backdoor attacks [24]. Here, we firstly, as an attacker, trained TrojanNet with the CIFAR10 image classification as main task and Fashion-MNIST and MNIST classification as two hidden tasks. Given the TrojanNet is provided, a simple fine-tune the main task is carried out by the defender and continue the training of the TrojanNet using the CIFAR10 dataset for the other 100 epochs. The testing accuracy of each task is shown in Fig. 8. It is clear that the hidden tasks are completely removed/forgotten after about 50 epochs. The TrojanNet validated in Fig. 8 is with `float32` format to align with the original work [26]. We have also

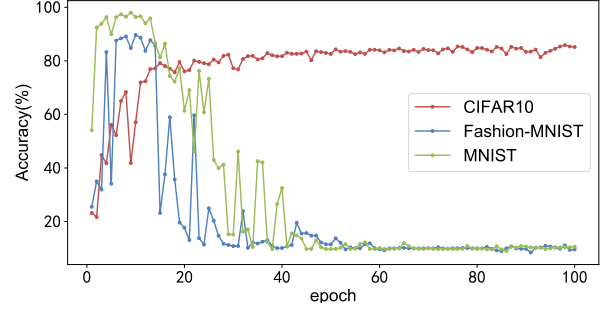


Figure 8: TrojanNet removal. By simply continuously training the TrojanNet with the known task, the hidden tasks are completely disrupted or removed after about 50 epochs.

tested this removal when the TrojanNet is BNN, which has the same removal effect. Therefore, we can conclude that the TrojanNet is easy to remove without affecting the main task that is known and deployed by the user, though it is hard to be detected.

## VII. CONCLUSION

We have proposed RBNN to further improve the memory utilization for resource-constrained IoT devices by  $\times M$ , with  $M$  as the number of tasks concurrently embedded. Notes that RBNN is built upon the ultimate binary quantization of DNN—the reconfigurable paradigm indeed does apply to non-binary neural networks. Comprehensive experiments validate the practicability and effectiveness of the RBNN by: i) up to 7 tasks trained over each of 3 popular model architectures; ii) tasks with varying number of classes; iii) tasks spanning distinct domains. More specifically, the task accuracy in the RBNN has no or only negligible degradation in comparison with standalone trained tasks. In addition, the RBNN naturally enables a novel paradigm of IP protection for model provider. The IP of each task integrated within RBNN can even be issued per user as well as per device, which greatly reduces the IP purchase for normal users while reserving the commercial benefits of the model provider.

## REFERENCES

- [1] A. Krizhevsky, I. Sutskever, and G. E. Hinton, “Imagenet classification with deep convolutional neural networks,” *Communications of the ACM*, vol. 60, no. 6, pp. 84–90, 2017.
- [2] F. N. Iandola, S. Han, M. W. Moskewicz, K. Ashraf, W. J. Dally, and K. Keutzer, “Squeezenet: Alexnet-level accuracy with 50x fewer parameters and <0.5 MB model size,” *arXiv preprint arXiv:1602.07360*, 2016.
- [3] K. He, X. Zhang, S. Ren, and J. Sun, “Deep residual learning for image recognition,” in *Proceedings of the IEEE Conference on Computer Vision and Pattern Recognition*, 2016, pp. 770–778.
- [4] K. Han, Y. Wang, Q. Tian, J. Guo, C. Xu, and C. Xu, “Ghostnet: More features from cheap operations,” in *Proceedings of the IEEE Conference on Computer Vision and Pattern Recognition*, 2020, pp. 1580–1589.
- [5] X. Zhang, X. Zhou, M. Lin, and J. Sun, “Shufflenet: An extremely efficient convolutional neural network for mobile devices,” in *Proceedings of the IEEE Conference on Computer Vision and Pattern Recognition*, 2018, pp. 6848–6856.
- [6] R. David, J. Duke, A. Jain, V. J. Reddi, N. Jeffries, J. Li, N. Kreeger, I. Nappier, M. Natraj, S. Regev *et al.*, “TensorFlow Lite Micro: Embedded machine learning on tinyml systems,” *arXiv preprint arXiv:2010.08678*, 2020.

- [7] (Janary 2021) Tensorflow lite. [Online]. Available: <https://www.tensorflow.org/lite>
- [8] I. Hubara, M. Courbariaux, D. Soudry, R. El-Yaniv, and Y. Bengio, "Binarized neural networks," *Advances in Neural Information Processing Systems*, vol. 29, pp. 4107–4115, 2016.
- [9] M. Rastegari, V. Ordonez, J. Redmon, and A. Farhadi, "Xnor-net: Imagenet classification using binary convolutional neural networks," in *European Conference on Computer Vision*. Springer, 2016, pp. 525–542.
- [10] A. Bulat and G. Tzimiropoulos, "XNOR-net++: Improved binary neural networks," in *British Machine Vision Conference (BMVC)*, 2019. [Online]. Available: <https://arxiv.org/abs/1909.13863>
- [11] B. Martinez, J. Yang, A. Bulat, and G. Tzimiropoulos, "Training binary neural networks with real-to-binary convolutions," in *International Conference on Learning Representations (ICLR)*, 2020. [Online]. Available: <https://arxiv.org/abs/2003.11535>
- [12] R. Andri, L. Cavigelli, D. Rossi, and L. Benini, "Yodann: An architecture for ultralow power binary-weight CNN acceleration," *IEEE Transactions on Computer-Aided Design of Integrated Circuits and Systems*, vol. 37, no. 1, pp. 48–60, 2017.
- [13] F. Conti, P. D. Schiavone, and L. Benini, "XNOR neural engine: A hardware accelerator IP for 21.6-fj/op binary neural network inference," *IEEE Transactions on Computer-Aided Design of Integrated Circuits and Systems*, vol. 37, no. 11, pp. 2940–2951, 2018.
- [14] H. Qin, R. Gong, X. Liu, X. Bai, J. Song, and N. Sebe, "Binary neural networks: A survey," *Pattern Recognition*, p. 107281, 2020.
- [15] Y. Zhang, J. Pan, X. Liu, H. Chen, D. Chen, and Z. Zhang, "FracBNN: Accurate and FPGA-efficient binary neural networks with fractional activations," in *The 2021 ACM/SIGDA International Symposium on Field-Programmable Gate Arrays*, 2021, pp. 171–182.
- [16] S. Ruder, "An overview of multi-task learning in deep neural networks," *arXiv preprint arXiv:1706.05098*, 2017.
- [17] N. Lin, X. Chen, H. Lu, and X. Li, "Chaotic weights: A novel approach to protect intellectual property of deep neural networks," *IEEE Transactions on Computer-Aided Design of Integrated Circuits and Systems*, DOI: 10.1109/TCAD.2020.3018403, 2020.
- [18] Y. Adi, C. Baum, M. Cisse, B. Pinkas, and J. Keshet, "Turning your weakness into a strength: Watermarking deep neural networks by backdooring," in *27th {USENIX} Security Symposium ({USENIX} Security 18)*, 2018, pp. 1615–1631. [Online]. Available: <https://www.usenix.org/conference/usenixsecurity18/presentation/adi>
- [19] B. Darvish Rouhani, H. Chen, and F. Koushanfar, "Deepsigns: An end-to-end watermarking framework for ownership protection of deep neural networks," in *Proceedings of the Twenty-Fourth International Conference on Architectural Support for Programming Languages and Operating Systems*, 2019, pp. 485–497.
- [20] Y. Gao, C. Xu, D. Wang, S. Chen, D. C. Ranasinghe, and S. Nepal, "Strip: A defence against trojan attacks on deep neural networks," in *Proceedings of the 35th Annual Computer Security Applications Conference*, 2019, pp. 113–125.
- [21] S. Han, H. Mao, and W. J. Dally, "Deep compression: Compressing deep neural networks with pruning, trained quantization and Huffman coding," in *NIPS Deep Learning Symposium*, 2015. [Online]. Available: <https://arxiv.org/abs/1510.00149>
- [22] G. Hinton, O. Vinyals, and J. Dean, "Distilling the Knowledge in a Neural Network," *arXiv preprint arXiv:1503.02531*, 2015.
- [23] A. Polino, R. Pascanu, and D. Alistarh, "Model compression via distillation and quantization," in *International Conference on Learning Representations (ICLR)*, 2018. [Online]. Available: <https://arxiv.org/abs/1802.05668>
- [24] Y. Gao, B. G. Doan, Z. Zhang, S. Ma, A. Fu, S. Nepal, and H. Kim, "Backdoor attacks and countermeasures on deep learning: a comprehensive review," *arXiv preprint arXiv:2007.10760*, 2020.
- [25] E. Bagdasaryan and V. Shmatikov, "Blind backdoors in deep learning models," in *USENIX Security Symposium*, 2020. [Online]. Available: <https://arxiv.org/abs/2005.03823>
- [26] C. Guo, R. Wu, and K. Q. Weinberger, "Trojanet: Exposing the danger of trojan horse attack on neural networks," in *The International Conference on Learning Representations (ICLR)*, 2020. [Online]. Available: <https://openreview.net/forum?id=BJeGA6VtPS>
- [27] E. Bagdasaryan, A. Veit, Y. Hua, D. Estrin, and V. Shmatikov, "How to backdoor federated learning," in *International Conference on Artificial Intelligence and Statistics*. PMLR, 2020, pp. 2938–2948.
- [28] S. Shan, E. Wenger, B. Wang, B. Li, H. Zheng, and B. Y. Zhao, "Gotta catch'em all: Using honeypots to catch adversarial attacks on neural networks," in *Proceedings of the ACM SIGSAC Conference on Computer and Communications Security*, 2020, pp. 67–83.
- [29] D. M. Sommer, L. Song, S. Wagh, and P. Mittal, "Towards probabilistic verification of machine unlearning," *arXiv preprint arXiv:2003.04247*, 2020.
- [30] G. Hinton, N. Srivastava, and K. Swersky, "Neural networks for machine learning," *Coursera, video lectures*, vol. 264, no. 1, 2012.
- [31] Y. LeCun, L. Bottou, Y. Bengio, and P. Haffner, "Gradient-based learning applied to document recognition," *Proceedings of the IEEE*, vol. 86, no. 11, pp. 2278–2324, 1998.
- [32] H. Xiao, K. Rasul, and R. Vollgraf, "Fashion-mnist: a novel image dataset for benchmarking machine learning algorithms," *arXiv preprint arXiv:1708.07747*, 2017.
- [33] Y. Netzer, T. Wang, A. Coates, A. Bissacco, B. Wu, and A. Y. Ng, "Reading digits in natural images with unsupervised feature learning," 2011. [Online]. Available: [http://ufldl.stanford.edu/housenumbers/nips2011\\_housenumbers.pdf](http://ufldl.stanford.edu/housenumbers/nips2011_housenumbers.pdf)
- [34] A. Krizhevsky, G. Hinton *et al.*, "Learning multiple layers of features from tiny images," Citeseer, Tech. Rep., 2009. [Online]. Available: <http://citeseerx.ist.psu.edu/viewdoc/download?doi=10.1.1.222.9220&rep=rep1&type=pdf>
- [35] Z. Liu, P. Luo, X. Wang, and X. Tang, "Deep learning face attributes in the wild," in *Proceedings of International Conference on Computer Vision (ICCV)*, December 2015, pp. 3730–3738.
- [36] P. Warden, "Speech Commands: A Dataset for Limited-Vocabulary Speech Recognition," *ArXiv e-prints*, Apr. 2018. [Online]. Available: <https://arxiv.org/abs/1804.03209>
- [37] K. Simonyan and A. Zisserman, "Very deep convolutional networks for large-scale image recognition," *arXiv preprint arXiv:1409.1556*, 2014.
- [38] Z. Liu, Z. Shen, M. Savvides, and K.-T. Cheng, "Reactnet: Towards precise binary neural network with generalized activation functions," in *European Conference on Computer Vision*. Springer, 2020, pp. 143–159.
- [39] A. Bulat, B. Martinez, and G. Tzimiropoulos, "Bats: Binary architecture search," in *European Conference on Computer Vision (ECCV)*, 2020. [Online]. Available: <https://arxiv.org/abs/2003.01711>
- [40] L. Geiger and P. Team, "Larq: An open-source library for training binarized neural networks," *Journal of Open Source Software*, vol. 5, no. 45, p. 1746, Jan. 2020. [Online]. Available: <https://doi.org/10.21105/joss.01746>
- [41] N. Parmar, A. Vaswani, J. Uszkoreit, L. Kaiser, N. Shazeer, A. Ku, and D. Tran, "Image transformer," in *International Conference on Machine Learning*. PMLR, 2018, pp. 4055–4064.
- [42] H. Zhang, I. Goodfellow, D. Metaxas, and A. Odena, "Self-attention generative adversarial networks," in *International Conference on Machine Learning*. PMLR, 2019, pp. 7354–7363.
- [43] Y. Gao, S. F. Al-Sarawi, and D. Abbott, "Physical unclonable functions," *Nature Electronics*, vol. 3, no. 2, pp. 81–91, 2020.
- [44] C. Gu, W. Liu, Y. Cui, N. Hanley, M. O'Neill, and F. Lombardi, "A flip-flop based arbiter physical unclonable function (APUF) design with high entropy and uniqueness for FPGA implementation," *IEEE Transactions on Emerging Topics in Computing*, DOI: 10.1109/TETC.2019.2935465, 2019.
- [45] Y. Gao, Y. Su, L. Xu, and D. C. Ranasinghe, "Lightweight (reverse) fuzzy extractor with multiple reference PUF responses," *IEEE Transactions on Information Forensics and Security*, vol. 14, no. 7, pp. 1887–1901, 2018.
- [46] B. Wang, Y. Yao, S. Shan, H. Li, B. Viswanath, H. Zheng, and B. Y. Zhao, "Neural cleanse: Identifying and mitigating backdoor attacks in neural networks," in *2019 IEEE Symposium on Security and Privacy (SP)*. IEEE, 2019, pp. 707–723.
- [47] H. Chen, C. Fu, J. Zhao, and F. Koushanfar, "Deepinspect: A black-box trojan detection and mitigation framework for deep neural networks," in *Proceedings of the 28th International Joint Conference on Artificial Intelligence*. AAAI Press, 2019, pp. 4658–4664.